Numerical investigation of fully developed turbulent fluid flow and heat transfer in a square duct

Hyon Kook Myong
Air Conditioning and Environmental Control Laboratory,
Korea Institute of Science and Technology, Seoul, Korea

Three-dimensional fully developed turbulent fluid flow and heat transfer in a square duct are numerically investigated with the author's anisotropic low-Reynolds-number k-ε turbulence model. Special attention has been given to the regions close to the wall and the corner, which are known to influence the characteristics of secondary flow a great deal. Hence, instead of the common wall function approach, the no-slip boundary condition at the wall is directly used. Velocity and temperature profiles are predicted for fully developed turbulent flows with constant wall temperature. The predicted variations of both local wall shear stress and local wall heat flux are shown to be in close agreement with available experimental data. The present paper also presents the budget of turbulent kinetic energy equation and the systematic evaluation for existing wall function forms. The commonly adopted wall function forms that are valid for two-dimensional flows are found to be inadequate for three-dimensional turbulent flows in a square duct.

Keywords: turbulence; anisotropic k-ε model; secondary flow; heat transfer; wall function; prediction

Introduction

Turbulent flows commonly encountered in engineering practice occur in straight noncircular ducts; examples include heat exchangers, nuclear reactors, turbomachinery, and air-conditioning systems. These flows are characterized by the occurrence of secondary flows in the cross-sectional plane, which results from the anisotropy of Reynolds normal stresses in the cross-sectional plane induced by the three-dimensionality of the flow.[1,2] Although the magnitude of turbulence-driven secondary motion is only of the order of 2–3 percent of the streamwise mean velocity, this motion causes the streamwise mean velocity and temperature fields to be distorted considerably toward the corners and thus can have important consequences. For example, both the local wall shear stress and the local wall heat flux along the duct periphery are dominated by the presence of this secondary flow, which causes these variables to increase initially toward the corner. This behavior is of great importance for phenomena such as sediment transport and erosion problems. Therefore, it is important, from a design standpoint, to be able to predict local fluid flow and heat transfer behavior accurately in straight noncircular ducts.

A considerable number of experimental investigations have primarily been concerned with the influence of duct geometry on the overall behavior of skin friction and heat transfer rate. The earlier experiments indicated that empirical equations for these quantities could be closely related to correlations derived for turbulent flow in circular pipes (secondary flows do not exist there) through the concept of a hydraulic diameter. More extensive later studies have shown, however, that flow and heat transfer behavior are considerably geometry dependent, and hence the duct geometry needs to be considered in detail.[3,4] In addition, if local values of the wall shear stress and/or wall heat flux are used in the correlation for each position around the periphery, the frequently adopted assumption that the velocity and temperature profiles can be described by the usual inner logarithmic law of the wall developed for two-dimensional (2-D) flows also lacks experimental verification, particularly in both the corner and wall regions where there are still little available experimental data due to the difficulty of experimental measurement.

Since the secondary flow in a straight noncircular duct is caused by turbulence as discussed previously, this particular flow situation provides a natural vehicle for examining the validity of existing turbulence models. Thus, a theoretical analysis of the problem should take account of the secondary motions, for example, in order to calculate the behavior of skin friction and heat transfer rate accurately. In an early theoretical analysis, however, no mechanism for the development of secondary flow was taken into account,[5] and consequently both predicted local wall shear stress and wall heat flux distributions did not show experimentally observed behavior. The widely used (isotropic) k-ε model also has no built-in mechanism for the development of secondary flow due to its inherent isotropic characteristics, i.e., the stress and mean strain fields are co-aligned. For these reasons, most of the turbulence models developed for predicting these flows are essentially based on the Reynolds stress models, although they show considerable variation in the style of approach; examples include equilibrium models (e.g., a three-dimensional [3-D] length scale model by Gessner and Emery[6]), one-equation transport models,[7] two-equation transport models,[8] and algebraic stress models.[9–11] All of these models are, however, known to show quantitatively somewhat poor predictions of local wall shear stress and local wall heat flux distributions, although they predict qualitatively the correct trends as a whole.[6] It may be first anticipated that the discrepancy between predictions and experiments is caused

Address reprint requests to Dr. Myong at the Air Conditioning and Environmental Control Lab., Korea Institute of Science and Technology, P.O. Box 131, Cheongryang, Seoul 130-650, Korea.

Received 2 December 1990; accepted 3 May 1991

by deficiencies in the models, since all these models are simplified from the original forms of the Reynolds stress models with several assumptions that are questionable. This aspect has recently been systematically investigated by Demuren and Rodi[11] and Myong and Kobayashi.[12]

Another cause for the discrepancies between predictions and experiment seems to lie in the wall functions specified improperly by previous models. It is clear that this approach is less than desirable from the standpoint of numerical prediction, since both regions close to the wall and the corner are known to influence the characteristics of secondary flow a great deal. However, all of the previous models have, in fact, used the wall function approach as a wall boundary condition, partly because the near-wall modeling of Reynolds stress models is still far from complete. Up to the present, several forms of wall function have been proposed and used in the previous models, but their validity has not been verified, particularly for the near-corner region. Therefore, if predictions based on wall function approach are made, it is difficult to know whether discrepancies between predictions and experiment in both the near-wall and the near-corner regions are due to improperly specified wall functions or to deficiencies in the model itself. At the present time, no systematic evaluation for these wall function forms has appeared in the open literature. It is one main intent of this paper to present this evaluation.

Recently, the author[13–15] has proposed an anisotropic low-Reynolds-number k-ε turbulence model that is valid right up to the wall. This is just an extended form of its (isotropic) low-Reynolds-number k-ε model[13,16] but broadens the range of applicability while maintaining most of the popular features of the latter. This model has already been found capable of predicting the anisotropic normal Reynolds stresses up to the wall, with the correct wall-limiting behavior, and also proven to perform satisfactorily in several flow situations, including turbulent pipe and channel flows, 2-D boundary layer flows with and without pressure gradients, and even for developing 3-D turbulent flows in a square duct.[13,15] In addition, for developing 3-D turbulent flows in a square duct, it is found that the performance of the present model, including the anisotropic normal Reynolds stresses and distributions of U, k, and $\overline{uv}$, is by no means inferior to that of the previous higher-order models (e.g., Demuren and Rodi[11]).[12]

In the present paper, the author's anisotropic low-Reynolds-number k-ε model is used to predict 3-D fully developed turbulent fluid flow and heat transfer in a square duct as the simplest geometry in which secondary flows arise. We will not use the wall function approach but will use the no-slip condition at the wall, since the turbulence structure in regions close to the wall and the corner are known to govern the secondary flow generation mechanism, and also the evaluation of wall function forms is one main intent of the present paper. The resulting set of equations is simplified only by the boundary-layer approximations and solved with a forward marching numerical procedure for 3-D shear layers until fully developed flow is attained.

It should be noted that the present paper goes beyond the experimental investigation by paying particular attention to the predictions in regions close to the corner and the wall, where little experimental data have been reported due to the difficulty of experimental measurement. Since the turbulence structure in regions close to the wall and the corner are known to govern the secondary flow generation mechanism as mentioned previously, it is desirable to obtain information on these regions. Also, the present predictions provide a body of material that future modelers and experimenters may wish to compare with their own results.

Mathematical model

Reynolds averaged Navier-Stokes equations

The Reynolds averaged Navier-Stokes equations governing the distribution of the mean velocity and temperature components

Notation

a	Duct half width (Figure 1)
a'	Diagonal half width (Figure 1)
C_1, C_2, C_3	Turbulence model constants for anisotropy
C_f	Friction factor ($C_f \equiv 2\bar{\tau}_w/(\rho U_b^2)$)
$C_{\varepsilon 1}, C_{\varepsilon 2}, C_\mu$	Turbulence model constants
D	Hydraulic diameter (Figure 1)
f_μ, f_2	Modification functions in k-ε model
h	Heat transfer coefficient
k	Thermal conductivity or turbulent kinetic energy
Nu	Nusselt number ($\mathrm{Nu} \equiv hD/k$)
P	Mean static pressure or turbulent kinetic energy production
Pr	Prandtl number
Pr_t	Turbulent Prandtl number
$\dot{q}, \bar{\dot{q}}$	Local and average wall heat flux, respectively
Re	Reynolds number ($\mathrm{Re} \equiv U_b D/\nu$)
R_t	Turbulent Reynolds number ($\mathrm{R}_t \equiv \mathrm{k}^2/(\nu\varepsilon)$)
T	Mean temperature
T^+	Dimensionless temperature
t	Fluctuating component of temperature
$\overline{u^2}, \overline{v^2}, \overline{w^2}$	Reynolds normal stress components
$\overline{uv}, \overline{uw}, \overline{vw}$	Reynolds shear stress components
u_τ	Friction velocity ($u_\tau \equiv \sqrt{\tau_w/\rho}$)
U^+	Dimensionless velocity ($U^+ \equiv U/u_\tau$)
U, V, W	Mean velocity components (Figure 1)
V'	Mean velocity component along diagonal
x, y, z	Cartesian coordinates (Figure 1)
y'	Cartesian coordinate along diagonal (Figure 1)
y^+, z^+	Dimensionless wall coordinate ($y^+ \equiv u_\tau y/\nu$)

Greek symbols

α	Thermal diffusivity
δ_{ij}	Kronecker delta
κ	von Karman's constant
ν	Kinematic viscosity
ν_t	Eddy diffusivity of momentum
ρ	Density
$\sigma_k, \sigma_\varepsilon$	Turbulence model constants for diffusion of k and ε
ε	Dissipation rate of k
$\tau_w, \bar{\tau}_w$	Local and average wall shear stress, respectively

Subscripts

b	Bulk-mean
c	Center
w	Wall

in a straight duct may be written as follows:

Continuity equation:

$$\frac{\partial U}{\partial x}+\frac{\partial V}{\partial y}+\frac{\partial W}{\partial z}=0 \tag{1}$$

Streamwise (or longitudinal) momentum equation:

$$U\frac{\partial U}{\partial x}+V\frac{\partial U}{\partial y}+W\frac{\partial U}{\partial z}$$
$$=-\frac{1}{\rho}\frac{\overline{dP}}{dx}-\frac{\overline{\partial uv}}{\partial y}-\frac{\overline{\partial uw}}{\partial z}+\nu\left(\frac{\partial^2 U}{\partial y^2}+\frac{\partial^2 U}{\partial z^2}\right) \tag{2}$$

Momentum equations governing the secondary velocities V and W:

$$U\frac{\partial V}{\partial x}+V\frac{\partial V}{\partial y}+W\frac{\partial V}{\partial z}$$
$$=-\frac{1}{\rho}\frac{\partial P}{\partial y}-\frac{\overline{\partial v^2}}{\partial y}-\frac{\overline{\partial vw}}{\partial z}+\nu\left(\frac{\partial^2 V}{\partial y^2}+\frac{\partial^2 V}{\partial z^2}\right) \tag{3}$$

$$U\frac{\partial W}{\partial x}+V\frac{\partial W}{\partial y}+W\frac{\partial W}{\partial z}$$
$$=-\frac{1}{\rho}\frac{\partial P}{\partial z}-\frac{\overline{\partial vw}}{\partial y}-\frac{\overline{\partial w^2}}{\partial z}+\nu\left(\frac{\partial^2 W}{\partial y^2}+\frac{\partial^2 W}{\partial z^2}\right) \tag{4}$$

Thermal energy equation:

$$U\frac{\partial T}{\partial x}+V\frac{\partial T}{\partial y}+W\frac{\partial T}{\partial z}$$
$$=-\frac{\overline{\partial vt}}{\partial y}-\frac{\overline{\partial wt}}{\partial z}+\alpha\left(\frac{\partial^2 T}{\partial y^2}+\frac{\partial^2 T}{\partial z^2}\right) \tag{5}$$

The coordinate system and pertinent variables used in the present paper are shown in Figure 1. It is noted that, using the boundary-layer approximations, the streamwise momentum and heat fluxes have been neglected, and the pressure gradient $\partial P/\partial x$, originally appearing in Equation 2, has been replaced by the cross-sectional average pressure gradient $\overline{dP/dx}$, following the method of Patankar and Spalding.[17] The viscous stress terms appearing in the momentum and thermal energy equations are not neglected, since, in the present calculation procedure, the no-slip boundary condition at the wall is directly used in place of the common wall function approach as mentioned previously.

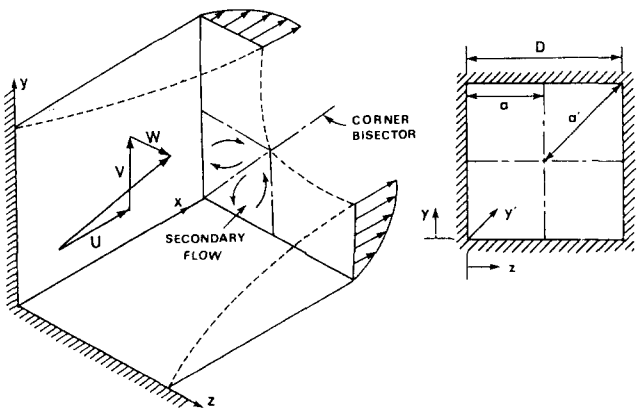

Figure 1 Coordinate system and pertinent variables

Turbulence model

As a turbulence model for determining the Reynolds stresses appearing in the previously given momentum equations, the author's anisotropic low-Reynolds-number k-ε turbulence model[12,13,15] is introduced in the present study. With the boundary-layer approximations, the transport equations of k and ε, and each Reynolds stress component are expressed as follows[12]:

$$U\frac{\partial k}{\partial x}+V\frac{\partial k}{\partial y}+W\frac{\partial k}{\partial z}=\frac{\partial}{\partial y}\left[\left(\nu+\frac{\nu_t}{\sigma_k}\right)\frac{\partial k}{\partial y}\right]+\frac{\partial}{\partial z}\left[\left(\nu+\frac{\nu_t}{\sigma_k}\right)\frac{\partial k}{\partial z}\right]+P-\varepsilon \tag{6}$$

$$U\frac{\partial \varepsilon}{\partial x}+V\frac{\partial \varepsilon}{\partial y}+W\frac{\partial \varepsilon}{\partial z}=\frac{\partial}{\partial y}\left[\left(\nu+\frac{\nu_t}{\sigma_\varepsilon}\right)\frac{\partial \varepsilon}{\partial y}\right]+\frac{\partial}{\partial z}\left[\left(\nu+\frac{\nu_t}{\sigma_\varepsilon}\right)\frac{\partial \varepsilon}{\partial z}\right]+C_{\varepsilon 1}\frac{\varepsilon}{k}P-C_{\varepsilon 2}f_2\frac{\varepsilon^2}{k} \tag{7}$$

where

$$P=-\overline{uv}\frac{\partial U}{\partial y}-\overline{uw}\frac{\partial U}{\partial z}-\overline{v^2}\frac{\partial V}{\partial y}-\overline{w^2}\frac{\partial W}{\partial z} \tag{8}$$

$$\overline{u^2}=\frac{2}{3}k+\frac{1}{3}\nu_t\frac{k}{\varepsilon}(2C_1-C_3)\left[\left(\frac{\partial U}{\partial y}\right)^2+\left(\frac{\partial U}{\partial z}\right)^2\right]+2\nu\frac{k}{\varepsilon}\left[\left(\frac{\partial\sqrt{k}}{\partial y}\right)^2+\left(\frac{\partial\sqrt{k}}{\partial z}\right)^2\right] \tag{9}$$

$$\overline{v^2}=\frac{2}{3}k-2\nu_t\frac{\partial V}{\partial y}-\frac{1}{3}\nu_t\frac{k}{\varepsilon}\left[(C_1-2C_3)\left(\frac{\partial U}{\partial y}\right)^2+(C_1+C_3)\left(\frac{\partial U}{\partial z}\right)^2\right]-\nu\frac{k}{\varepsilon}\left[\frac{4}{3}\left(\frac{\partial\sqrt{k}}{\partial y}\right)^2+\frac{2}{3}\left(\frac{\partial\sqrt{k}}{\partial z}\right)^2\right] \tag{10}$$

$$\overline{w^2}=\frac{2}{3}k-2\nu_t\frac{\partial W}{\partial y}-\frac{1}{3}\nu_t\frac{k}{\varepsilon}\left[(C_1-2C_3)\left(\frac{\partial U}{\partial z}\right)^2+(C_1+C_3)\left(\frac{\partial U}{\partial y}\right)^2\right]-\nu\frac{k}{\varepsilon}\left[\frac{4}{3}\left(\frac{\partial\sqrt{k}}{\partial z}\right)^2+\frac{2}{3}\left(\frac{\partial\sqrt{k}}{\partial y}\right)^2\right] \tag{11}$$

$$\overline{uv}=-\nu_t\frac{\partial U}{\partial y},\qquad \overline{uw}=-\nu_t\frac{\partial U}{\partial z} \tag{12,13}$$

$$\overline{vw}=-\nu_t\left(\frac{\partial W}{\partial y}+\frac{\partial V}{\partial z}\right)+C_3\nu_t\frac{k}{\varepsilon}\left(\frac{\partial U}{\partial y}\right)\left(\frac{\partial U}{\partial z}\right) \tag{14}$$

$$\nu_t=C_\mu\sqrt{k}L=C_\mu f_\mu\frac{k^2}{\varepsilon} \tag{15}$$

$$f_\mu=(1+3.45/\sqrt{R_t})[1-\exp(-y^+/70)] \tag{16}$$

$$f_2=\{1-(2/9)\exp[-(R_t/6)^2]\}[1-\exp(-y^+/5)]^2 \tag{17}$$

$$\sigma_k=1.4,\ \sigma_\varepsilon=1.3,\ C_{\varepsilon 1}=1.4,\ C_{\varepsilon 2}=1.8,\ C_\mu=0.09 \tag{18}$$

In the previous equations, two model constants C_1 and C_3 are given as 0.8 and -0.15, respectively, which are the same values

as those proposed previously for boundary-layer flows.[14,15] It should be recognized here that, contrary to the previous Reynolds (or algebraic) stress models, the present anisotropic model is substantially derived from the standard (isotropic) k-ε turbulence model, i.e., the standard k-ε model is obtained in the limit as $C_i \to 0$, and is directly applicable up to the wall.[12,15] Note that, in deriving Equations 8–14, terms that are quadratic in the secondary flow velocity components have been neglected since they are small. Note also that the wall coordinate y^+ appearing in the modification functions of Equations 16 and 17 denotes the wall coordinate using the minimum value between distances from each wall (for more details see Reference 12).

To close the thermal energy equation of Equation 5, we approximate, following long-established practice with the k-ε model, the turbulent heat flux $-\overline{u_i t}$ by using the concept of the turbulent Prandtl number as follows:

$$\overline{vt} = -\frac{\overline{uv}}{\mathrm{Pr}_t}\frac{\partial T/\partial y}{\partial U/\partial y}, \qquad \overline{wt} = -\frac{\overline{uw}}{\mathrm{Pr}_t}\frac{\partial T/\partial z}{\partial U/\partial z} \tag{19,20}$$

The turbulent Prandtl number is specified as a constant value in order to close the thermal energy equation.

Solution procedure and boundary conditions

For a given bulk Reynolds number, Equations 1–4 and 6–18 are solved numerically in order to predict the developing and fully developed velocity field. This solution is then coupled with Equations 5, 19, and 20 to predict the local temperature field using constant values for the turbulent Prandtl number under the assumption of constant properties. Since all the differential equations introduced previously are parabolic in the streamwise direction, an efficient forward-marching solution procedure can be employed. In the present study, a revised version of the 3-D parabolic finite difference procedure of Patankar and Spalding[17] is employed; in particular, the SIMPLER algorithm of Patankar[18] is substituted for the original SIMPLE algorithm in an attempt to improve its rate of convergence. At the inlet cross-section of the duct, a uniform distribution of all variables is prescribed, i.e., the secondary velocities V and W are set to zero, and the turbulent kinetic energy is given based on the experimental data. The dissipation rate ε is given a small value such that the eddy diffusivity ν_t is several times the molecular viscosity ν. Starting from these initial conditions, the step-by-step integration is undertaken until fully developed flow with no profile change in the streamwise direction is attained. More detailed information on the solution procedure is given elsewhere.[12]

The forward step size is initially 0.01 percent of the channel hydraulic diameter D but was enlarged progressively to a maximum level of 1 percent of D. At each step several iterations are carried out to reduce the residuals to negligible levels. The mesh typically comprises 66 × 66 grid points distributed non-uniformly over a cross-sectional quadrant: the clustering function stretches the mesh in y- and z-directions by using the geometric progression, and three to four grid lines are, at least, within $y^+ < 5$. These are concentrated in the sublayer and buffer regions near the wall. Validation of the numerical procedure is achieved through comparisons between the numerical results with different grid spacing and forward step sizes.

Boundary conditions are prescribed at symmetry planes and at solid walls. At symmetry planes, the velocity component normal to the symmetry plane is equal to zero, while for all other quantities the gradients normal to this plane are taken as zero. At the solid walls, all of the velocities and Reynolds stresses are equal to zero at the wall, and the dissipation rate at the wall is set equal to $\nu(\partial^2 k/\partial y^2)_w$ or $\nu(\partial^2 k/\partial z^2)_w$.

To obtain the heat transfer characteristics of the flow, we must solve, in addition to the hydrodynamic and turbulence properties discussed previously, the energy conservation equation. The heat transfer field is solved for the case where the average circumferential surface flux is uniform along the duct and the circumferential wall temperature is constant.

Results and discussion

Fluid flow field

The predicted distributions of the friction coefficient C_f for fully developed flow in a square duct are compared with the experimental data[3,19–21] in Figure 2. From the figure it can be seen that the present predictions agree quite well with the experimental results over a wide range of Reynolds numbers. It is informative to mention that, in the present model the average wall shear stress $\overline{\tau}_w$ is calculated directly from the local wall shear stress $\tau_w = \mu(\partial U/\partial y)_w$, as will be discussed below. Therefore, the present results seem likely to indicate the adequacy of the present model for near-wall turbulence, since this affects strongly C_f.

Figure 3 shows the isovel contours of U/U_c for the fully developed flow, along with the experiment.[22] The predicted isovel of streamwise mean velocity shows the typical bulging toward the corner, which is caused by the secondary motion. Close comparison of the predicted distributions with the experimental results indicates that the predictions agree quite well with the data, although they show a little less bulging of the velocity contours toward the corner.

The predicted contours of turbulent kinetic energy for fully developed flow in a square duct, which are normalized by U_c^2, are shown in Figure 4 along with the experimental data of Fujita et al.[22] The predicted results are in close agreement with the measurements, displaying faithfully the distortion of the contours toward the corner as a result of movement of high momentum fluid near the center outward along the diagonal, although they show a little less bulging toward the corner than the experimental data. The prediction and the experiment, however, share the fact that distortions of turbulent kinetic energy contours are more pronounced that those of the isovels of streamwise velocity. It should be also valuable to note that the present model shows clearly the distribution pattern of turbulent kinetic energy in regions close to the corner and the wall: the maximum value of turbulent kinetic energy occurs in the near-wall region far from the corner.

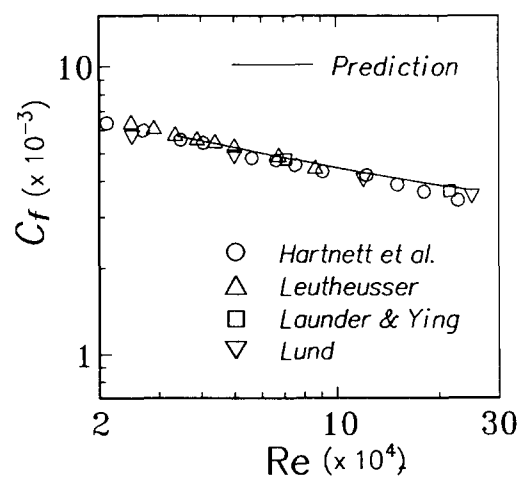

Figure 2 Friction coefficient for fully developed flow in a square duct

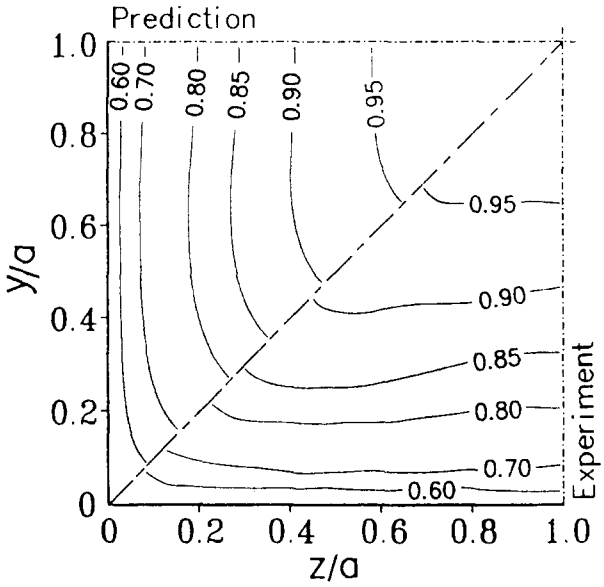

Figure 3 Contours of streamwise mean velocity U/U_c at $x/D = 84$ (Re = 65,000, experiment; Fujita et al.[22])

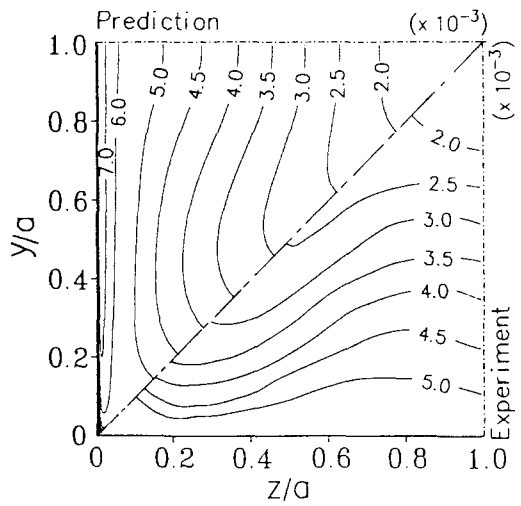

Figure 4 Contours of turbulent kinetic energy k/U_c^2 (Re = 65,000, experiment; Fujita et al.[22])

Figure 5 shows the predicted local wall shear stress variations for fully developed flow in a square duct along with the experimental data.[21,22] Experimental data indicate that the wall shear stress first rises from the symmetry plane toward the corner, with the peak shear stress about midway between the corner and the mid-point of the duct sides, and then falls again near the corner, approaching zero at the corner. It was reported by Gessner and Emery[6] that all previous models tend to overpredict shear stress away from the corners and underpredict values in the near-corner region. The present model, however, simulates the previously mentioned experimental behavior well. Also, from Figure 5 the present results show the tendency of the secondary motion to smooth out variations in wall shear stress around the perimeter of the duct, which is a little more pronounced at the higher Reynolds number.

A more complete comparison between predictions and available experimental data for developing flows has been recently presented elsewhere.[12] Also, the details of model performance on the local structure of turbulence and other systematic discussions of the contours of the important turbulence quantities for fully developed flows are reported elsewhere.[23]

Heat transfer field

The Nusselt number dependence on Reynolds number for fully developed flow and heat transfer in a square duct is shown in Figure 6, along with the experimental data.[4,24,25] The present prediction with the turbulent Prandtl number of 0.9 agrees fairly well with the experimental data over a wide range of Reynolds number and the prediction with $Pr_t = 1.0$ is also acceptable. It should be noted here that the computations were performed for both constant wall heat flux and constant wall temperature conditions, but there are no substantial differences between the Nusselt number results for fully developed flow.

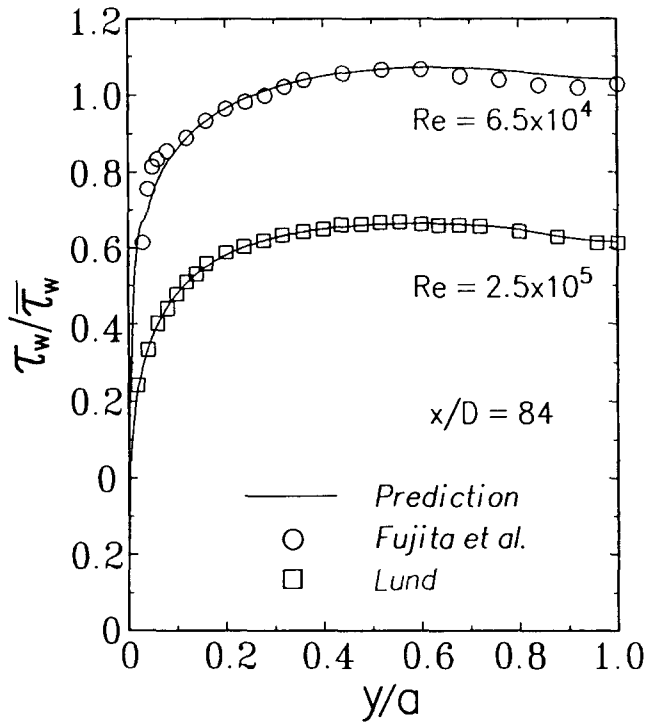

Figure 5 Local wall shear stress variations for fully developed flow

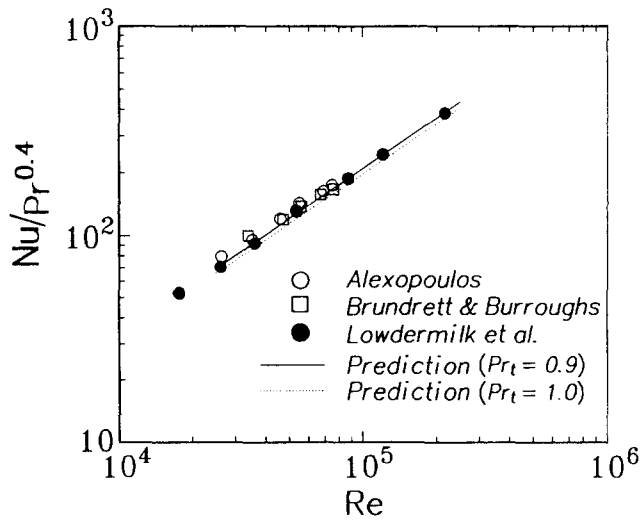

Figure 6 Nusselt number dependence on Reynolds number for fully developed flow

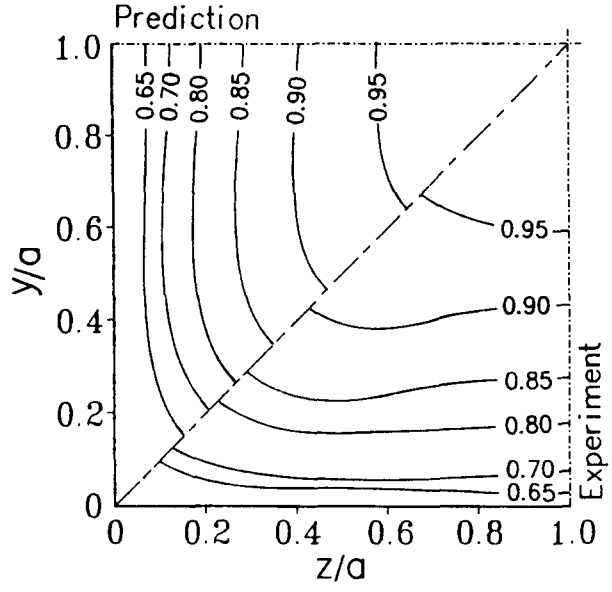

Figure 7 Temperature contours of $(T_w - T)/(T_w - T_c)$ at $x/D = 96$ (Re = 75,000, experiment; Alexopoulos[24])

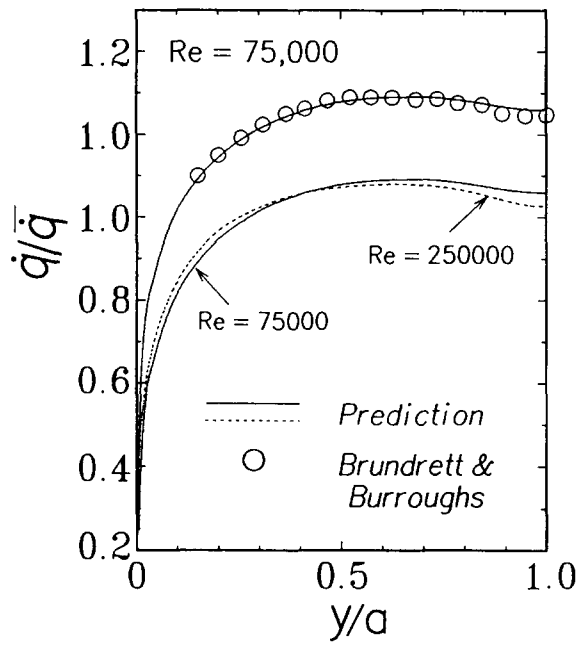

Figure 8 Local wall heat flux variations for fully developed flow

Figure 7 shows the predicted temperature contours of $(T_w - T)/(T_w - T_c)$ for fully developed flow in a square duct with a constant wall temperature with the experimental data.[24] It can be seen clearly that the isotherms display a similar pattern to the isovels shown in Figure 3. This is expected since the differential equations and boundary conditions for momentum and energy transport have close similarity, although they are not identical. A close comparison of predicted isovels and isotherms in the near-corner region, however, indicates that the secondary flow does not convect thermal energy as effectively as primary flow momentum.

The predicted and measured local wall heat flux variations around the perimeter of the square duct are compared in Figure 8. The present predictions are in excellent agreement with the experimental data of Brundrett and Burroughs[4]: both show that the maximum wall heat flux occurs about midway between the corner and the mid-point of the sides. A comparison between predictions for Re = 75,000 and Re = 250,000 also indicates that a slight Reynolds number effect is present; the tendency of the secondary motion to smooth out variations in wall heat flux around the perimeter of the duct is more pronounced at the higher Reynolds number.

Budget of turbulent kinetic energy transport

The transport process of turbulent kinetic energy is of great importance to understanding the turbulence mechanism, but such details would not be readily available from experiments, particularly for complex turbulent flows in a square duct. Thus, it is of great interest to investigate numerically the details on the transport process of turbulent kinetic energy. The turbulent kinetic energy equation shown in Equation 6 can be rearranged as follows:

$$\underbrace{-\left(U\frac{\partial k}{\partial x}+V\frac{\partial k}{\partial y}+W\frac{\partial k}{\partial z}\right)}_{\text{Convection}}+\underbrace{\frac{\partial}{\partial y}\left[\left(\nu+\frac{\nu_t}{\sigma_k}\right)\frac{\partial k}{\partial y}\right]}_{\text{Diffusion}}+\frac{\partial}{\partial y}\left[\left(\nu+\frac{\nu_t}{\sigma_k}\right)\frac{\partial k}{\partial y}\right]+\underbrace{P}_{\text{Production}}-\underbrace{\varepsilon}_{\text{Dissipation}}=0 \quad (21)$$

Figure 9 shows the predicted contours of the individual terms in Equation 21, which are normalized by U_b^3/D. From the figure, it can be first understood that both rates of convection and diffusion are one order of magnitude less than those of production and dissipation as generally expected. It can be also seen that the production rate and the dissipation rate are nearly balanced and consequently that local equilibrium between them prevails throughout the duct cross region except at the core region, where the production obviously vanishes and the dissipation rate is balanced with the diffusion rate. The present results demonstrate clearly the local equilibrium assumption that is commonly adopted in the case of theoretical analysis as will be discussed in the following section.

Evaluation of wall function approach

When the wall function approach is employed in a two-transport equation model or in an algebraic stress model, the following three conditions for the variation of U, k, and e are generally specified along the first mesh line adjacent to a boundary wall as wall functions, namely

$$\frac{U}{u_\tau}=\frac{1}{\kappa}\ln\frac{yu_\tau}{\nu}+\mathrm{C} \quad \text{or} \quad \frac{U}{u_\tau}=\frac{1}{\kappa}\ln(\mathrm{E}y^+) \quad (22)$$

$$\frac{k}{u_\tau^2}=\frac{\sqrt{\mathrm{F_p}}}{\sqrt{\mathrm{C}_\mu}}, \qquad \frac{\varepsilon y}{u_\tau^3}=\frac{\mathrm{F_p}}{\kappa_1} \quad (23,24)$$

where κ, C, E, and C_μ are prescribed constants with $F_p = 1$ and $\kappa = \kappa_1$ for 2-D flows. Up to the present time, most numerical investigators still predict 3-D turbulent flow in a square duct by applying Equations 22–24 in a given transverse plane along the first mesh line (say, y = constant) between the corner bisector ($z = y$) and the wall bisector ($z = a$) at each streamwise location. Recently, however, Gessner[26] has reported on experimental measurements by Eppich that, although Equation 22 fits fairly well by the near-wall data, k/u_τ^2 and $\varepsilon y/u_\tau^3$ vary in the near-wall and the near-corner regions, so that Equations 23 and 24 are not satisfied when F_p and κ_1 are prescribed as constants. Demuren and Rodi[11] have also asserted that, for a wall normal to z, the boundary conditions for k and

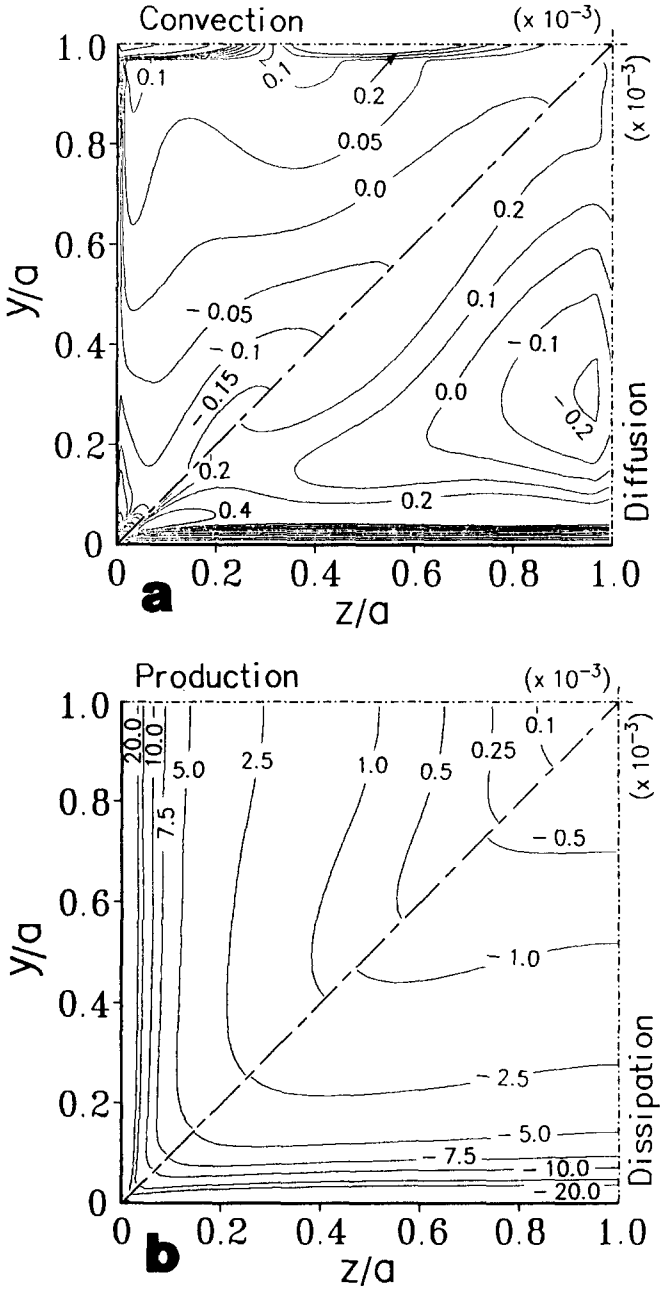

Figure 9 Budget of turbulent kinetic energy equation (normalized by U_b^3/D). (*a*) The rates of convection and diffusion. (*b*) The rates of production and dissipation

ε are given with $\kappa = \kappa_1$ and

$$F_p = 1 + \left(\frac{\partial U}{\partial y}\right)^2 \Big/ \left(\frac{\partial U}{\partial z}\right)^2 \qquad (25)$$

Note that for a wall normal to y, z and y must be exchanged. Since F_p takes a value of 2 at the corner bisector and unity at the wall bisector, respectively, Equations 23 and 24 imply that the ratios k/u_τ^2 and $\varepsilon y/u_\tau^3$ increased the corner.

Figure 10 shows the predicted inner-law velocity profiles at four positions in the z direction, which are normalized by the local wall friction velocities at each position. It is generally known from experimental evidence that the velocity profiles can be described by the usual inner logarithmic law of the wall of Equation 22 developed for 2-D flows, with a little scatter in the involved constants, but not universal defect laws are found for the outer region. The present predictions confirm clearly the experimental evidence, but indicate that the usual inner logarithmic law of the wall is not valid over the somewhat wide range of the corner region.

The predicted variations of k and ε at two positions in the y direction are shown in Figures 11 and 12, respectively, along with the experimental data presented by Gessner[26] and Demuren and Rodi's relations using Equations 23 and 24 with F_p given by Equation 25. Note that the results shown in Figures 11 and

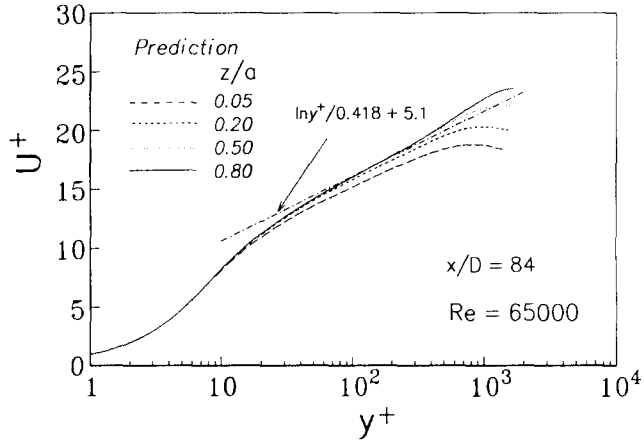

Figure 10 Inner-law velocity profiles for fully developed flow

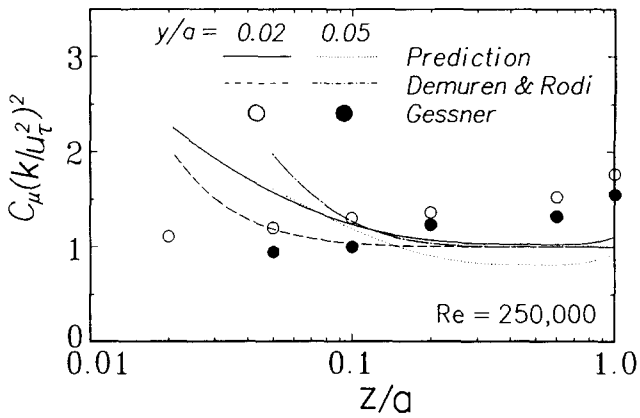

Figure 11 Predicted variations of k at two positions in the y-direction

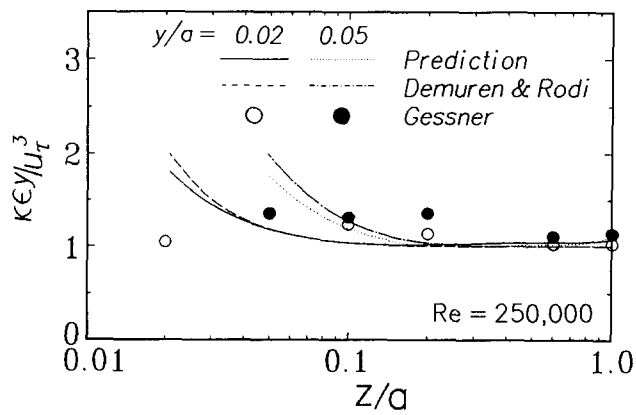

Figure 12 Predicted variations of ε at two positions in the y-direction

12 denote the variations of F_p and F_p/κ_1, respectively. It is first evident that the commonly adopted boundary conditions of Equations 23 with $F_p = 1$, implying that the production is equal to twice the dissipation at the corner, are not in accord with reality. The predicted variations of F_p and F_p/κ_1 show a similar trend to the relation of Equation 25 with $\kappa = \kappa_1$, which is asserted by Demuren and Rodi,[11] although slight quantitative discrepancies exist in the corner region. In contrast, the measurements reported by Gessner,[26] however, show the opposite trend: the ratio of k to u_τ^2 (or F_p) decreases as the corner is approached. This trend is apparently in conflict with the notion of local equilibrium arguments leading to Equation 25, since F_p of Equation 25 can be derived from the assumptions of both logarithmic law of the wall and local equilibrium in consideration of the fact that the generation of turbulent kinetic energy P given by Equation 8 is influenced by the presence of both walls in the corner region, while u_τ and y relate only to the wall nearest to the point in question. Hence, F_p ensures that both the production and the dissipation of turbulent kinetic energy are balanced even in the near-corner region. This fact is confirmed by the present result as shown in Figure 9. Demuren and Rodi[11] reported that this trend could only be explained by a fairly strong convective transport of k by the secondary motion from the core region with lower k into the corner. The present prediction, however, does not support this assertion as shown in Figure 9.

The large discrepancy near the corner between the experiment[26] and Demuren and Rodi's relations (and/or the present predictions) may be mainly traced to the following facts: in their development of wall functions for k and ε of Equations 23 and 24, Demuren and Rodi started by assuming that $-\overline{uv}/u_\tau^2 = 1$ in the region bounding the wall $y = 0$, which is also commented by one of the reviewers. The present model also predicts that $-\overline{uv}/u_\tau^2$ has approximately unit value in the whole region bounding the wall $y = 0$. In contrast, the experimental data show that $-\overline{uv}/u_\tau^2$ decreases from unity on the wall bisector to a value of approximately 0.5 on the corner bisector (e.g., see Figure 12 in Reference 27). This fact can be also indirectly found elsewhere (e.g., Figure 9 in Reference 12): the present model predicts fairly well the local primary shear stress $-\overline{uv}$ along the wall bisector, but overpredicts it along the corner bisector, although its absolute value along the corner bisector is much lower than that along the wall bisector in the region bounding the wall $y = 0$. Note that there is still little definite explanation of this experimental evidence. Thus, although more extensive theoretical and experimental investigations should be required to clarify this point, it might be understood that turbulent flows in the immediate vicinity of a corner still cannot be predicted with good accuracy even with the aid of the present anisotropic k-ε model.

Figure 13 shows the predicted inner-law temperature profiles at four positions in the z-direction. It is evident from Figure 13 that the inner-law temperature profiles display much the same pattern as the inner-law velocity profiles shown in Figure 10: the present predictions clearly support the experimental evidence, but the usual inner logarithmic law of the wall is not valid over the fairly wide range of the corner region.

Conclusion

Using the anisotropic low-Reynolds-number k-ε turbulence model, 3-D turbulent fluid flow and heat transfer in a square duct are numerically predicted. In contrast to previous models, the present model has used directly the no-slip boundary condition at the wall in place of the common wall function approach. In addition, the resulting set of equations are simplified only by the boundary-layer assumptions. Both temperature and velocity field predictions for fully developed flow display the transport effects of secondary flow and are in general agreement with the experimental evidence. Local wall shear stress and wall heat flux distributions exhibit excellent agreement with observed peaking behavior between the duct midplane and corner region. The predicted averaged friction factor and Nusselt number behavior are found to be in good agreement with the data.

In addition, the budget of turbulent kinetic energy equation and the systematic evaluation of existing wall function forms are presented in this paper. The present result demonstrates clearly the local equilibrium assumption commonly adopted in the case of theoretical analysis. It is also found that the commonly adopted wall function forms, which are valid for 2-D flows, are inadequate for 3-D turbulent flows.

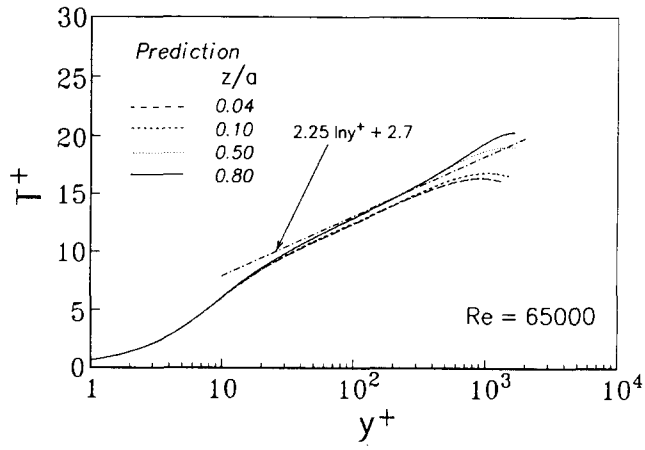

Figure 13 Inner-law temperature profiles for fully developed flow

Acknowledgments

The present work was mainly undertaken at both the Institute of Industrial Science (IIS) and Research Center for Advanced Science and Technology (RCAST) of the University of Tokyo. The author gratefully acknowledges the support of both IIS and RCAST. The author is also grateful to Professors N. Kasagi, T Kobayashi, and M. Hirata at the University of Tokyo for many helpful conversations.

References

1 Brundrett, E., and Baines, W. D. The production and diffusion of vorticity in duct flow. *J. Fluid Mech.*, 1964, **19**, 375–394

2 Perkins, H. J. The formation of streamwise vorticity in turbulent flow. *J. Fluid Mech.*, 1970, **44**, 721–740

3 Leutheusser, H. J. Turbulent flow in rectangular ducts. *J. Hydraulics Div., Proc. ASCE*, 1963, **89**(HY3), 1–19

4 Brundrett, E., and Burroughs, P. R. The temperature inner-law and heat transfer for turbulent air flow in a vertical square duct. *Int. J. Heat Mass Transfer*, 1967, **10**, 1133–1142

5 Deissler, R. G., and Taylor, M. F. Analysis of turbulent flow and heat transfer in non-circular passages. *NASA Tech. Rep.*, R-31, 1959

6 Gessner, F. B., and Emery, A. F. The numerical prediction of developing turbulent flow in rectangular ducts. *Trans. ASME J. Fluids Eng.*, 1981, **103**, 445–455

7 Launder, B. E., and Ying, W. M. Prediction of flow and heat transfer in ducts of square cross-section. *Proc. Inst. Mech. Engrs.*, 1973, **187**, 455–461

8 Ramachandra, V., and Spalding, D. B. Fluid flow and heat transfer in rectangular sectioned ducts. Report HTS/76/21, Dept. of Mech. Eng., Imperial College of Science and Technology, London, 1976

9 Naot, D., Shavit, H., and Wolfshtein, M. Numerical calculation of Reynolds stresses in a square duct with secondary flow. *Wärme-und Stoffübertragung*, 1974, **7**, 1787–1806

10 Nakayama, A., Chow, W. L., and Sharma, D. Calculation of fully developed turbulent flows in ducts of arbitrary cross-section. *J. Fluid Mech.*, 1983, **128**, 199–217

11 Demuren, A. O., and Rodi, W. Calculation of turbulence-driven secondary motion in non-circular ducts. *J. Fluid Mech.*, 1984, **140**, 189–222

12 Myong, H. K., and Kobayashi, T. Numerical simulation of three-dimensional developing turbulent flow in a square duct with the anisotropic k-ε model. Presented at the 1st Joint ASME-JSME Fluids Eng. Conf., June 23–27, 1991, Portland, OR, USA; also FED-Vol. 117, Advances in Numerical Simulation of Turbulent Flows, ASME, 1991, 17–23

13 Myong, H. K. Fundamental Studies on Two-Equation Turbulence Model for Numerical Predictions of Wall-Bounded Shear Flow and Heat Transfer. Dr. Eng. Thesis, The University of Tokyo, Tokyo, Japan, 1988

14 Myong, H. K., and Kasagi, N. A proposal for an anisotropic k-ε turbulence model satisfying the wall-limiting condition of turbulence. *Trans. Japan Soc. Mech. Engrs.* (in Japanese) 1990, **56B**, 3298–3304

15 Myong, H. K., and Kasagi, N. Prediction of anisotropy of the near-wall turbulence with an anisotropic low-Reynolds-number k-ε turbulence model. *Trans. ASME J. Fluids Eng.*, 1990, **112**, 521–524

16 Myong, H. K., and Kasagi, N. A new approach to the improvement of k-ε turbulence model for wall-bounded shear flows. *JSME Int. J.*, Ser. II 1990, **33**, 63–72

17 Patankar, S. V., and Spalding, D. B. A calculation procedure for heat, mass and momentum transfer in 3-d parabolic flows. *Int. J. Heat Mass Transfer*, 1972, **15**, 1787–1806

18 Patankar, S. V. *Numerical Heat Transfer and Fluid Flow*. Hemisphere, New York, 1980

19 Hartnett, J. P., Koh, J. C. Y., and McComas, S. T. A. A comparison of predicted and measured friction factors for turbulent flow through rectangular ducts. *Trans. ASME J. Heat Transfer*, 1962, **84**, 82–88

20 Launder, B. E., and Ying, W. M. Secondary flow in ducts of square cross section. *J. Fluid Mech.*, 1972, **54**, 289–295

21 Lund, E. G. Mean flow and turbulence characteristics in the near corner region of a square duct. MS Thesis, Dept. of Mech. Eng., University of Washington, Seattle, WA, USA, 1977

22 Fujita, H., Yokosawa, H., Iwata, S., and Takahama, H. Turbulent flow in a square duct with roughened walls on two opposite sides (1st report, measurement of flow velocities and turbulent stresses). *Trans. Japan Soc. Mech. Engrs.* (in Japanese) 1986, **52B**, 3491–3497

23 Myong, H. K. Prediction of turbulence-driven secondary flow in a square duct with an anisotropic low-Reynolds-number k-ε model. Submitted to the *8th Symp. on Turbulent Shear Flows*, September 9–11, 1991, Munich, Germany

24 Alexopoulos, C. C. Temperature and velocity distributions and heat transfer for turbulent air flow in a square duct. M.A. Sc. Thesis, Dept. of Mech. Eng., University of Toronto, Ontario, Canada, 1964

25 Lowdermilk, W. H., Weiland, W. F., Jr, and Livingood, J. N. B. Measurement of heat transfer and friction coefficients for flows in noncircular ducts at high surface temperatures. *NACA RM*, E53J07, 1954

26 Gessner, F. B. Corner flow (secondary flow of the second kind). *Proc. 1980–1981 AFORS-HTTM Stanford Conf. on Complex Turbulent Flows*, edited by Kline, S. J., Cantwell, B., and Lilley, G. M., Stanford University, CA, USA, 1982

27 Gessner, F. B., Po, J. K., and Emery, A. F. Measurements of developing turbulent flow in a square duct. *Turbulent Shear Flows I*, Durst, et al., eds. Springer-Verlag, New York, 1979, 119–136